JCIM JOURNAL OF CHEMICAL INFORMATION AND MODELING

pubs.acs.org/jcim Article

Exploring the Conformers of an Organic Molecule on a Metal Cluster with Bayesian Optimization

Lincan Fang, Xiaomi Guo, Milica Todorović, Patrick Rinke, and Xi Chen*

Cite This: J. Chem. Inf. Model. 2023, 63, 745−752 Read Online

ACCESS | Metrics & More | Article Recommendations | Supporting Information

ABSTRACT: Finding low-energy conformers of organic molecules is a complex problem due to the flexibilities of the molecules and the high dimensionality of the search space. When such molecules are on nanoclusters, the search complexity is exacerbated by constraints imposed by the presence of the cluster and other surrounding molecules. To address this challenge, we modified our previously developed active learning molecular conformer search method based on Bayesian optimization and density functional theory. Especially, we have developed and tested strategies to avoid steric clashes between a molecule and a cluster. In this work, we chose a cysteine molecule on a well-studied gold−thiolate cluster as a model system to test and demonstrate our method. We found that cysteine conformers in a cluster inherit the hydrogen bond types from isolated conformers. However, the energy rankings and spacings between the conformers are reordered.

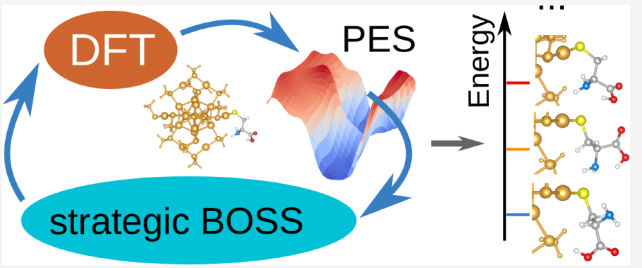

INTRODUCTION

Organic−inorganic hybrid systems composed of a metal core and organic molecules have become increasingly important in modern nanotechnology. The physical and chemical properties of the organic−inorganic heterostructures are highly tunable by, e.g., engineering the metal core, the molecules, and the molecule−metal interfaces. Their potential applications include catalysis,[1] molecular sensors,[2] bioimaging,[3] and nanomedicine.[4] However, hybrid material design and optimization remain fundamentally challenging because the desired properties often depend on the microscopic structure of the system, which is typically unknown.

Computational simulations, especially density functional theory (DFT), have proven essential for microscopic structure determinations of hybrid systems as they can accurately predict the structure on an atomic level, which experiments often cannot resolve. For a given molecule−cluster system, atomic models of the metal part and metal−molecule interface can be built from experimental data (e.g., electron microscopy),[5] previous reported crystal structures,[6] chemical intuition,[7] or data-driven methods.[8] However, the configurations of adsorbed molecules are difficult to determine.

Finding low-energy molecular conformers in the gas phase is already a challenging problem. Organic molecules are usually flexible and have a high-dimensional structural search space with many local minima. In addition, to accurately predict structures and energies of molecular conformers, costly quantum mechanical accuracy is required.[9] To address this conformer-search challenge, a variety of methods and tools such as systemic methods,[10] stochastic methods,[11,12] hierarchical methods,[13,14] and machine learning techniques[15−18] have been developed for molecular conformer search.

In recent years, Bayesian Optimization in combination with DFT has been widely applied to molecules and materials for structure search and property optimization.[19−21] In our recent work, we developed an active machine learning procedure for molecular conformer identification and ranking. We first fix the bond lengths and angles and choose the molecular dihedral angles as features to reduce the dimension of the search space. Then, we employ the Bayesian Optimization Structure Search (BOSS) code[19,22] to build a surrogate potential energy surface (PES) model in the reduced dimensions with iterative Bayesian Optimization (BO) sampling.[16] After the model converges, we extract the local minima from the surrogate PES and optimize the corresponding structures with DFT before adding free-energy contributions and quantum chemistry corrections. More details can be found in ref 16.

We have validated the accuracy and efficiency of our procedure on cysteine, serine, tryptophan, and aspartic acid.[16] However, the BOSS conformer search was not directly applicable to molecular conformers on a cluster, because close molecule−cluster contact or steric clashes could not be handled. If atoms in a structure come too close, the DFT

Received: September 5, 2022
Published: January 16, 2023

https://doi.org/10.1021/acs.jcim.2c01120
J. Chem. Inf. Model. 2023, 63, 745−752

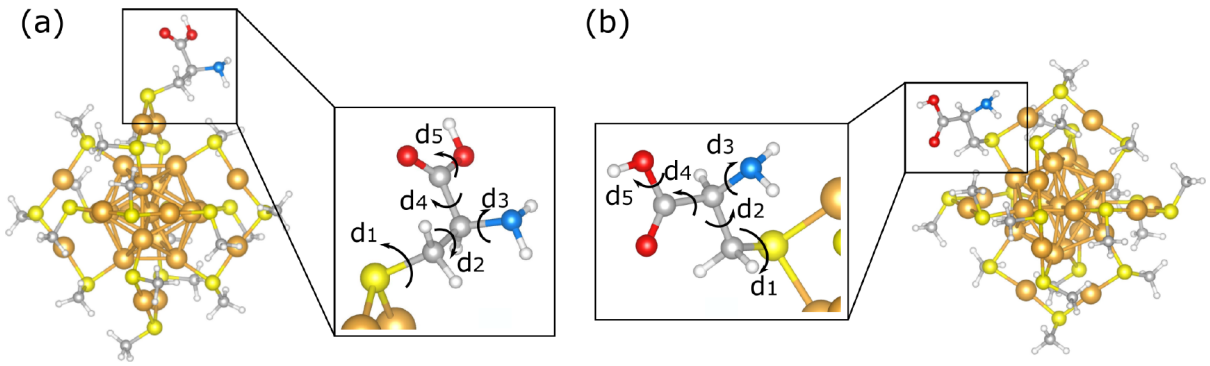

Figure 1. Ball−stick model of cysteine on $Au_{25}(SCH_3)_{17}$ cluster: (a) system A and (b) system B. Gold color is used for gold atoms, red for oxygen, white for hydrogen, gray for carbon, blue for nitrogen, and yellow for sulfur. d_1, d_2, d_3, d_4, and d_5 label the five dihedral angles of cysteine that we use to define our search space.

energy diverges or the DFT code returns an error, which means that no data point is returned to continue the iterative algorithm. This presents a problem in active learning. It leads to large model uncertainties and causes the acquisition function to repeatedly query the unphysical region of the search space. In this work, we developed strategies to address steric clashes in active learning by constructing different solutions in the regions where energy data could not be evaluated.

We used a cysteine molecule adsorbed on a well-studied thiolate-protected Au_{25} cluster[6,23] as a model system to test and demonstrate our method. We chose the system for several reasons. First, it offers us an ideal situation of cysteine in a complicated, confined environment. Second, the cluster contains a Au_{13} icosahedral core, protected by six SCH_3-Au-SCH_3-Au-SCH_3 V-shaped staples.[6,23] Consequently, cysteine can adsorb at two inequivalent S sites: one on the top of the V-shape staple, and the other on the side, as shown in Figure 1a and b. This allows us to study how the different surrounding environments affect the structures of cysteine. Third, we can compare to cysteine conformers in the gas phase from our previous study[16] to elucidate confinement and proximity effects.

In brief, we used a cysteine on a gold−thiolate cluster as a model system to develop and test strategies for avoiding steric clashes in BOSS active learning in the Methods section. In the Results and Discussion section, we compared the different strategies and applied the optimal one to investigate how the gold−thiolate cluster affects the structures and energy rankings of the cysteine conformers.

METHODS

Our procedure contains three steps: (i) system preparation, (ii) BOSS strategic structure search, and (iii) refinement, in analogy with the procedure we had developed for the molecular conformer search in the gas phase.[16]

In step (i), we first build an atomic model of the $Au_{25}(SCH_3)_{17}$(Cys) (Cys: cysteine) by replacing one SCH_3 in the well-studied $Au_{25}(SCH_3)_{18}$ cluster with a deprotonated cysteine molecule. SCH_3 was chosen here to reduce the computational cost and the complexity. We optimized this structure with DFT and set the total energy of the optimized structure as the energy reference 0 eV for the BOSS sampling in the next step. Since we are interested in searching the configurations of cysteine here, we adopt the "building block" concept.[19,24] Except for the atoms in cysteine, all other atoms are constrained during the machine learning procedure. As in our previous work,[16] we choose dihedral angles as the most informative degrees of freedom to describe the different cysteine configurations and refer to the dihedral angle space as *phase space*. The bond lengths and angles are fixed at their optimized values during BOSS sampling, because they are relatively rigid. Cysteine has two nonequivalent bonding sites on the $Au_{25}(SCH_3)_{17}$ cluster as illustrated in Figure 1a and b. We consider both of them and refer to them as system A and system B in the rest of the paper (Figure 1).

In step (ii), we employ BOSS to actively learn the PES of the system by BO iterative sampling. Each sample point contains dihedral angles d_i (i = 1, 2, 3, 4, 5) of cysteine (Figure 1) and the corresponding energy of $Au_{25}(SCH_3)_{17}$(Cys).

For small molecules in the gas phase, each dihedral angle contributes 360° to the full phase space (discounting possible rotational symmetries). This angular range might be restricted for a molecule on a cluster. Configurations that lead to steric clashes typically have a high energy and are therefore not important in the search for global minima, but they present a challenge to active learning. DFT calculations either crash for steric clashes or they return unfavorably high energies. The inability to sample a region of the search space leads to large uncertainties in the surrogate model, promoting explorative sampling and causing the active learning algorithm to repeatedly query this, ultimately irrelevant, part of the search space. Even if a DFT computation could proceed, including very high energies into the energy landscape produces a large model variance. This makes the model less accurate in the low-energy PES regions of interest, which then requires more sampling to refine.

To address these technical challenges, we devised and tested three different strategies to prevent sampling nonphysical structures. In strategy **i**, we try to identify a continuous region in phase space that is free of steric clashes. BOSS then samples only in this restricted phase space. In strategy **ii**, we define a "safe minimum distance" D_0 between any two atoms in the system to preselect physically meaningful structures. If the shortest distance between the cysteine and other atoms is longer than D_0, the energy of the structure will be calculated by DFT, otherwise a constant energy will be returned. In strategy **iii**, we use a logarithmic energy transformation to suppress high energy regions and apply an energy penalty to nonphysical structures for which DFT cannot return an energy. We discuss the details of the strategies and their advantages and limitations below.

https://doi.org/10.1021/acs.jcim.2c01120
J. Chem. Inf. Model. 2023, 63, 745−752

After the PES has been learned sufficiently well, in step (iii), we use the BOSS postprocessing routines to analyze the surrogate PES and extract the local minima configurations and related structures. In this step, we relax all degrees of freedom in the systems to refine the structures and energies.

The all-electron code FHI-aims[25−27] was applied for all DFT calculations. "Tight" numerical settings, "tier 2" basis sets for S, C, O, N, H, and the "tier 1" set for Au were used throughout. Following our previous work,[16] we used the Perdew−Burke−Ernzerhof (PBE) functional[28] with many-body dispersion corrections[29] in all DFT calculations. For structure optimizations, the geometry was considered to be converged when the maximum residual force (fmax) was below 0.01 eV/Å.

During the sampling, BOSS employed Gaussian process (GP) models to fit a surrogate PES to the data points, and then refined it by acquiring more data points at locations that minimize the exploratory lower confidence bound (eLCB) acquisition function. We applied a "rbf" kernel for the nonperiodic d_i in strategy **i** and a "stpd" kernel for the periodic d_i in strategies **ii** and **iii**.

In the interest of open science,[30,31] we make the results of all relevant calculations freely available on the Novel Materials Discovery (NOMAD) repository.[32]

Sampling in the Limited Phase Space. The most intuitive way to avoid steric clashes is to exclude those regions of phase space from sampling. To investigate whether such a "safe" region exists for our systems, we randomly generated 100,000 d_i (i = 1, 2, 3, 4, 5) structures for both systems A and B. Then, we calculated the shortest atomic pair distance D_{min} between cysteine and $Au_{25}(SCH_3)_{17}$ in each structure and plotted D_{min} against d_i in Figures S1−S3. If we limit the sampling range of d_1, there is a region where the cysteine and cluster will not become too close (Figure S1). However, we cannot exclude all the structures with steric clashes by restricting d_2, d_3, d_4, or d_5 (Figures S2−S3). The reason is that d_1 is the closest rotational bond to the cluster, thus determining the overall structure.

Figure 2a and b presents the d_1−d_2 2-D distribution of D_{min} for systems A and B. The panels suggest that we can obtain a "safe" sample region by restricting d_1 to [70°, 210°] for system A or [140°, 240°] for system B. In such a region, 99.7% of the structures have D_{min} > 1.0 Å; d_1 has a narrower "safe" region in system B than in system A due to the more restricted local environment. This strategy is easy to apply and very unlikely to sample the nonphysically meaningful structures, but it may miss parts of phase space that correspond to low-energy structures, such as the yellow areas to the left or the right of the red dashed region in Figure 2a and b.

Safe Distance Selection. In strategy **ii**, we address the clash problem by introducing a safe distance D_0 to classify "safe" and "unsafe" structures and treat them differently. If the shortest atomic distance D_{min} between the cysteine and the $Au_{25}(SCH_3)_{17}$ is larger than D_0, the structure will be identified as a physically meaningful one, and its energy will be its DFT energy E. Here, we chose D_0 equal to 1.4 Å, which lies around the typical bond length in organic molecules. In contrast, if D_{min} is smaller than D_0, the structure will be considered nonphysical, and no DFT calculation will be performed. Instead, a constant energy E_0 will be assigned to the structure. The energy E_{new} for updating the GP in BOSS sampling is

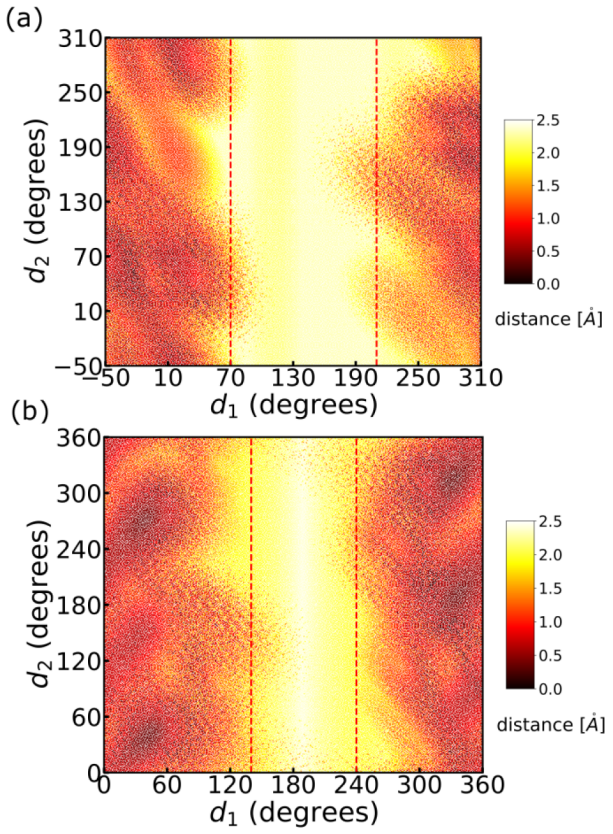

Figure 2. Two-dimensional (d_1 and d_2) maps of the shortest atomic pair distance D_{min} between cysteine and the cluster for (a) system A and (b) system B. In the plots, a light color means the structures have large D_{min}, while a dark color means the structures have small D_{min}, where the steric clash may happen. Strategy **i** only sampled d_1 between dashed red lines.

$$E_{new} = \begin{cases} E & D > D_0 \\ E_0 & D \le D_0 \end{cases} \quad (1)$$

In our tests, we tried constant and harmonic potentials for E_0. The agreement between the surrogate BOSS energy and DFT single-point energies for selected structures did not improve for harmonic potentials. Therefore, we discuss only constant potentials in this work. We tested E_0 = 2.0, 4.0, and 6.0 eV and found that the sampled structures have a similar energy distribution for system A (Figure S4). Therefore, we only present the results for E_0 = 6.0 eV here.

The advantage of strategy **ii** is its capacity to sample the entire phase space without performing DFT calculations for nonphysical structures. The disadvantages are that the surrogate PES is not accurate for structures with $D_{min} < D_0$, and the energy−structure relation is discontinuous around D_0 which could lead to suboptimal surrogate PES model fits. Since a structure with D_{min} smaller or close to D_0 typically has a high energy, these disadvantages should not affect the low-energy PES prediction.

Energy Transformation. In strategy **iii**, we introduce an energy cutoff E_{cut}. For a structure with a high DFT energy $E \ge E_{cut}$, we use a logarithmic energy transformation to attenuate the high energy of the nonphysical structure during BOSS sampling. In addition, for the structures where DFT simulations fail, we apply a penalty energy E_p to update the GP during BOSS sampling.

https://doi.org/10.1021/acs.jcim.2c01120
J. Chem. Inf. Model. 2023, 63, 745−752

$$E_{new} = \begin{cases} E & E \le E_{cut} \\ E_{cut} + log_{10}(E - E_{cut} + 1) & E > E_{cut} \\ E_p & \nexists E \end{cases} \quad (2)$$

We adopted E_{cut} = 2.0 eV and E_p = 4.5 eV in this work. Using E_{cut} = 1.0 or 3.0 eV did not change the main feature of E_{new} distribution (Figure S5). Strategy **iii** ensures a full phase space search and does not change the energy order of the structures where DFT calculations complete successfully. We employ smooth energy attenuation to bridge the landscape between high but chemically valid energies and the artificial energy penalty values and also to avoid introducing unphysical and sharp features into the model. The limitation is that the PES in the high-energy region is inaccurate, but this should not affect our low-energy structure search.

RESULTS AND DISCUSSION

We first monitor PES model convergence for the three strategies employed. Since our previous study on the 5-D or 6-D PES of amino acids showed that 1000 iterations are sufficient for learning their low-energy PES,[16] we sample the PES of system A with 1000 BOSS iterations. The hyperparameters length scales for BOSS GP fitting stabilized around 600, 600, and 800 iterations for strategies **i**, **ii**, and **iii**, as shown in Figure S6. Figure S7 illustrates the refinement of the predicted global minimum with iterative configurational sampling for the three strategies. Both the energy and the dihedral angles of the predicted global minimum conformer converged around iteration 200 for strategy **iii**, while the energy and the dihedral angles of the predicted global minimum converged around iteration 800 for using strategy **i** and strategy **ii**. From this analysis, we can conclude that our surrogate PES was sufficiently converged with 1000 iterations.

After 1000 BOSS iterations, we extracted the local minima locations and their related structures from the surrogate PES and refined the structures by DFT optimization. Then, we purged duplicate structures and only kept unique configurations ($\Delta d_{max} > 10°$ and $\Delta E > 0.0057$ eV). Using strategies **i**, **ii**, and **iii**, we finally obtained 37, 45, and 39 unique configurations within energy windows of 0.40, 0.68, and 0.63 eV from the global minimum, respectively.

We evaluated the strategies from two aspects: the accuracy of the surrogate PES and the energies of the final local minima structures we obtained. We picked the 30 lowest-energy structures after DFT relaxation for the evaluation. The accuracy of the surrogate PES is measured by the differences between the BOSS-predicted energies and the DFT single-point energies of the 30 structures before optimization. Figure 3a–c show that the DFT energy is generally higher than the BOSS-predicted energy for a given structure. The mean differences are 0.29, 1.14, and 0.52 eV for strategies **i**–**iii**. A smaller difference between the BOSS-predicted energy and the DFT single-point energy indicates that the surrogate PES is more accurate. From this perspective, strategies **i** and **iii** are better than strategy **ii**.

Systematic overestimation of BOSS minima values over DFT indicates a sharp variation of energy across the many peaks and minima in the interpolated surrogate model, but this is not relevant in our workflow. It is more important to retrieve the locations of the energy basins in the global landscape, which serve to initiate further local optimizations and compute local minima conformers.

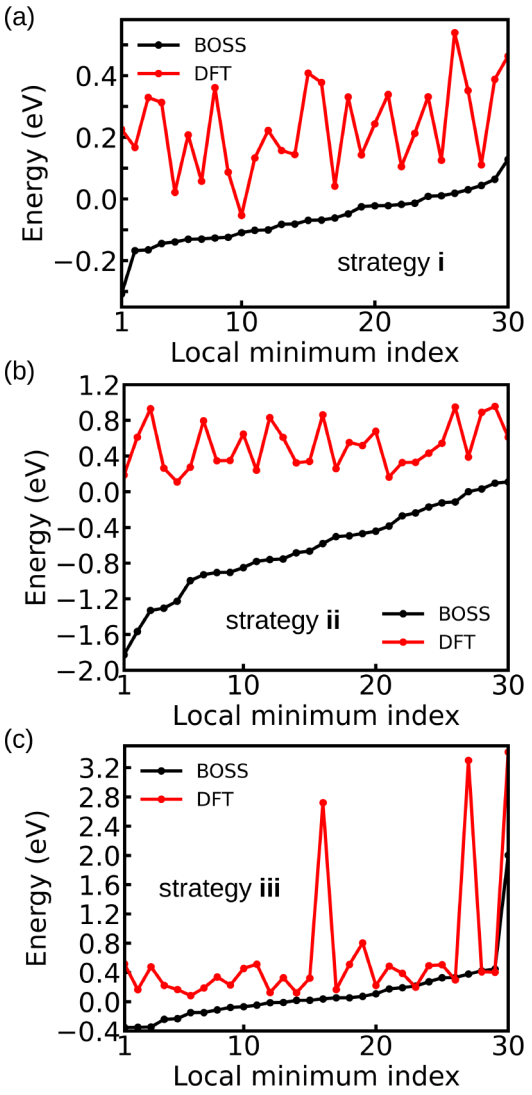

Figure 3. BOSS-predicted and DFT single-point energies of the 30 lowest-energy structures of system A with (a) strategy **i**, (b) strategy **ii**, and (c) strategy **iii**. The DFT energy of the atomic model we obtained in step (i) for the BOSS sampling was set to 0 eV.

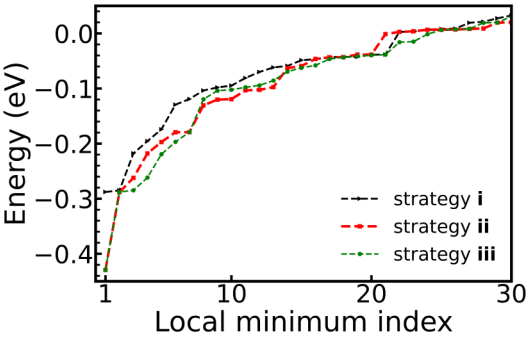

Figure 4. Relative energies of the 30 lowest-energy structures of system A after DFT optimization and removing duplicates. The DFT energy of the atomic model we obtained in step (i) for the BOSS sampling was set to 0 eV.

Figure 4 shows the energies of the 30 lowest-energy structures after DFT structure optimization. Overall the curves

https://doi.org/10.1021/acs.jcim.2c01120
J. Chem. Inf. Model. 2023, 63, 745–752

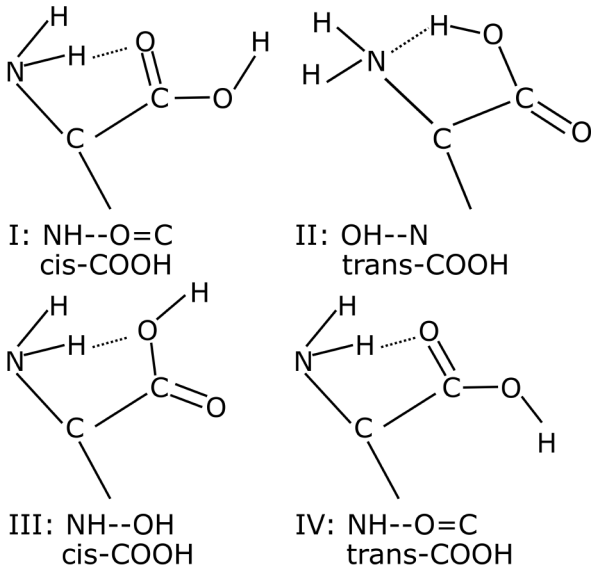

Figure 5. Types of hydrogen bonds between the amino group and the carboxyl group in cysteine.

generated by strategy **ii** and strategy **iii** are very close to each other, suggesting strategies **ii** and **iii** have obtained very similar local minima structures. In the higher energy region, the three curves are almost on top of each other, indicating the three strategies found the same structures in this energy region. However, in the low-energy region, the green curve lies below the other two, because strategy **iii** found more stable structures.

Strategy **i** missed the global minimum structure, while strategies **ii** and **iii** succeeded in finding it. This is because system A has low-energy regions which cannot be sampled in strategy **i** (i.e., any yellow area to the left or the right of the red dashed region in Figure 2). Unfortunately, the global minimum of system A falls into such an unsampled low-energy region. Overall, strategy **iii** exhibits the best performance, and we chose strategy **iii** to study system B.

Next, we present the results of an active learning structure search for systems A and B. We obtained 39 unique local minima structures for system A and 31 unique local minima structures for system B. These structures have the relative energy within 0.63 eV from global minimum in system A and within 0.40 eV in system B. Similar to the isolated cysteine molecule, internal hydrogen bonds are commonly formed in the low-energy structures of adsorbed cysteine. If we use a cutoff of r_{HB} = 3.5 Å to define a hydrogen bond, all the local minima structures within a relative energy of 0.34 eV from global minimum in system A and 0.35 eV in system B contain at least one intramolecular hydrogen bond in cysteine.

We assess how $Au_{25}(SCH_3)_{17}$ affects the configurations of cysteine and compare them to the isolated cysteine conformers. We choose the 11 cysteine conformers (Ia, Ib, I′b, IIa, IIb, IIc, III_{α}a, III_{α}b, III_{α}c, III_{β}b, III_{β}c), identified in ref 33 and our previous work ref 16, as the reference structures for comparison. The conformers were named I, II, and III depending on the type of hydrogen bond (Figure 5) and as

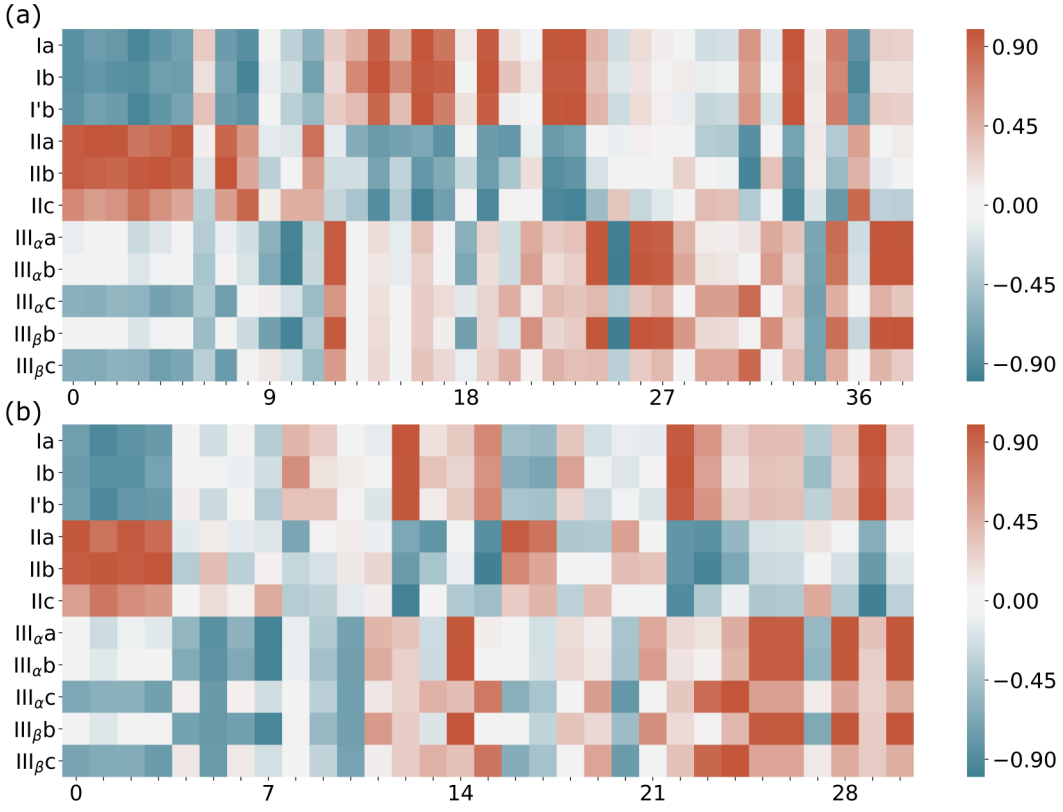

Figure 6. Similarity S_{cos} between the 11 reference cysteine conformers and the cysteine in the local minimum structures of (a) system A and (b) system B. The *y*-axis represents the 11 references; the *x*-axis lists the local minima structures of system A or system B in the increasing order of energy.

https://doi.org/10.1021/acs.jcim.2c01120
J. Chem. Inf. Model. 2023, 63, 745−752

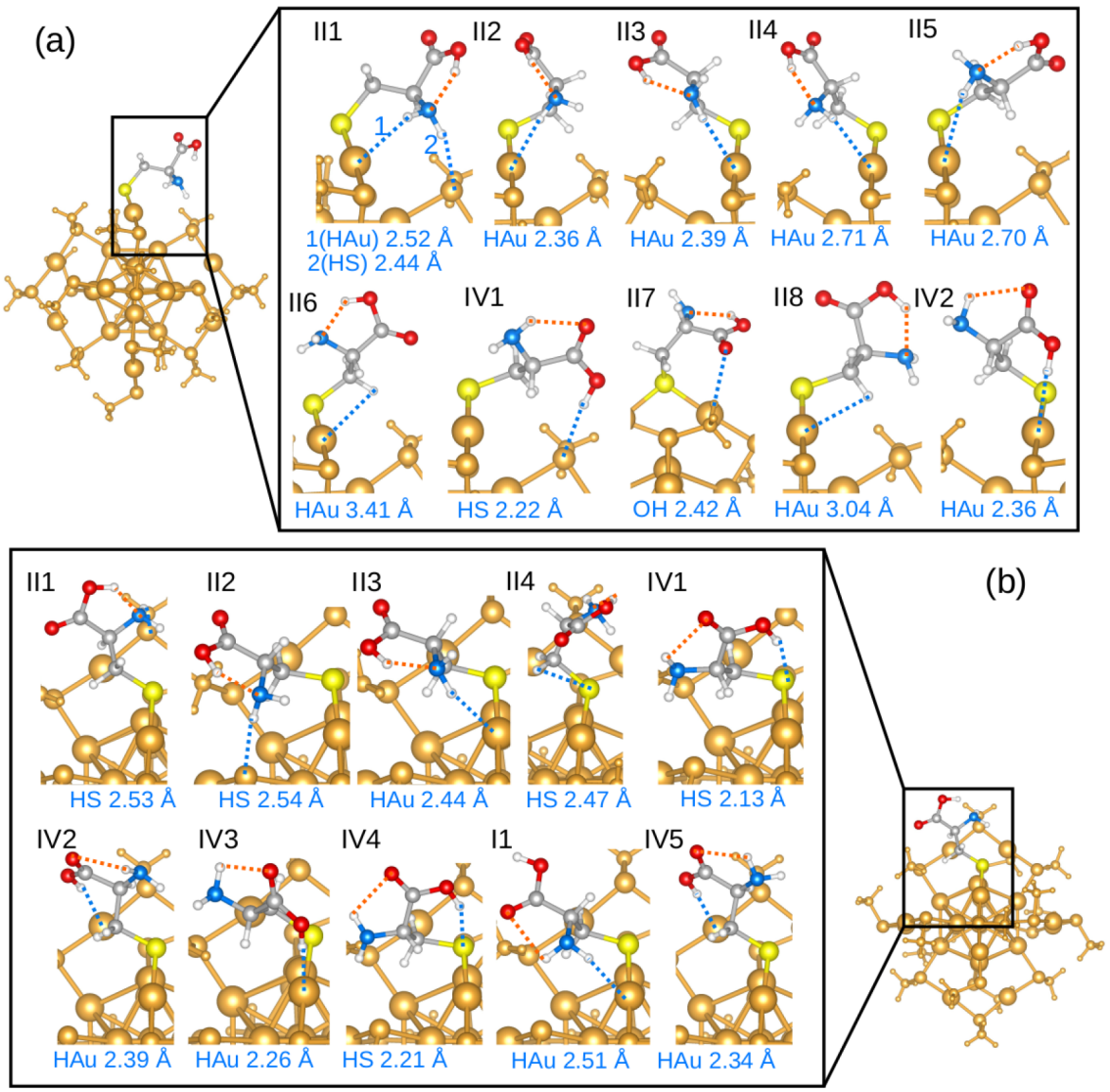

Figure 7. Predicted top ten low-energy conformers of system A (a) and system B (b) from the BOSS search.

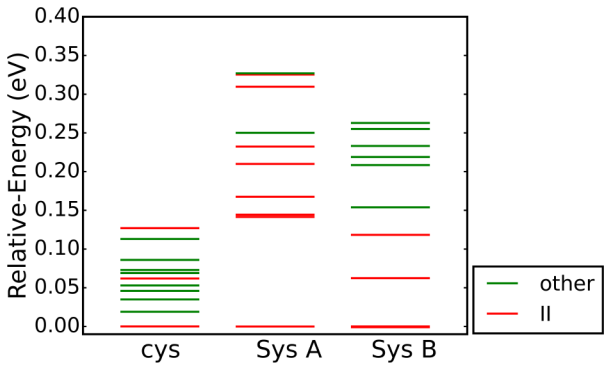

Figure 8. Relative energies of the ten most stable structures of cysteine molecules, system A, and system B. The red line means the structure contains a type II hydrogen bond in cysteine, while the green line means other types of hydrogen bonds in cysteine.

a, b, and c according to the configuration of the $-CH_2SH$ side chain.

The similarity of the two structures *a* and *b* can be measured with the following similarity index

$$S_{\cos} = \frac{\boldsymbol{v}_a \cdot \boldsymbol{v}_b}{|\boldsymbol{v}_a||\boldsymbol{v}_b|} \tag{3}$$

Here, v_a and v_b are the vectors $[\cos(d_2), \cos(d_3), \cos(d_4), \cos(d_5)]$ of the two structures (the definition of d_i is shown in Figure 1). Since d_1 has an ambiguous meaning among the molecule conformers and systems A and (the H atom binding to the S atom in cysteine molecule was replaced by a gold atom for the adsorbed molecule), we did not include d_1 in the similarity calculation. S_{cos} lies in the interval $[-1,1]$. The higher the value of S_{cos} is, the more similar the two structures are.

The S_{cos} of the cysteine configurations in systems A and B are plotted against the reference cysteine conformers in Figure 6a and b. Red colors indicate high similarity and blue low similarity. The red horizontal regions of high similarity in Figure 6 suggest that cysteine may form types I, II, and III hydrogen bonds when it adsorbs on $Au_{25}(SCH_3)_{17}$. However, there are local minima structures in systems A and B where the configurations of cysteine are not similar to any reference molecular conformers. After analysis, we found that most of these structures form a new type of hydrogen bond (NH−O═C hydrogen bond, trans-COOH configuration), which we named type IV (Figure 5).

https://doi.org/10.1021/acs.jcim.2c01120
J. Chem. Inf. Model. 2023, 63, 745−752

Figure 7a depicts the predicted 10 lowest-energy structures of system A. The orange dashed lines mark the hydrogen bonds, while the blue dashed lines indicate the shortest atomic distance between the cysteine and $Au_{25}(SCH_3)_{17}$. Eight out of the ten structures have type II hydrogen bonds, and two have type IV. Although structures II1−II8 all have the same kind of hydrogen bond, the energy varies by 0.33 eV, suggesting that the interactions between the cluster and cysteine play important roles in stabilizing the systems. In the structures shown in Figure 7a, the shortest distance between cysteine and the cluster is either from a hydrogen atom in the cysteine to a gold atom in the cluster or from a hydrogen atom in cysteine to a sulfur atom in the cluster. This suggests that the week H−Au and H−S interactions help to stabilize the system. These interactions could also explain why type IV hydrogen bonds do not exist in the reference cysteine conformers but often appear in systems A and B: the trans-COOH configurations facilitate the formations of the H−Au and H−S interactions.

Figure 7b depicts the predicted 10 lowest-energy structures of system B. The four lowest-energy structures have type II hydrogen bonds followed by four structures with type IV hydrogen bonds and one with type I. Similar to system A, the H−Au and H−S interactions help to stabilize the low-energy structures in system B. However, comparing Figure 7a and b, it is clear that the local environments significantly affect the energy ranking of the cysteine conformers on the cluster.

We plot the energies of the structures shown in Figure 7 in Figure 8 and include the energies of the top ten most stable gas-phase cysteine conformers. Comparing the energy ranking, we observe that systems A and B exhibit larger energy spacings between different configurations than the isolated cysteine molecular conformers. Second, type II hydrogen bonds are dominant in systems A and B. The structures within 0.15 eV from the global minimum of systems A and B all have type II hydrogen bonds. In contrast, for isolated cysteine, most conformers in the same energy window have other types of hydrogen bonds (types I and III). In addition, the energy difference between the lowest and the second-lowest structure is much larger in system A than in system B or in the isolated molecule. We attribute this difference to short H−S and H−Au distances we found in system A, but not in the other two.

CONCLUSION

In summary, we have developed three simple strategies to handle steric clashes during the active learning. We proposed an approach that combines the strategies with BO and DFT to search for low-energy structures of a molecule on a cluster. We chose a cysteine molecule on a well-studied gold−thiolate cluster as a model system to test and demonstrate our method. Based on the tests in this work, we recommend an "energy transformation" strategy that suppresses high energies with a logarithmic transformation and applies an energy penalty to nonphysical structures where DFT computations fail. This strategy results in a smooth BOSS simulation and effective learning of the low-energy region of the PES. However, for a system whose physical and nonphysical areas in phase space can be well separated by restricting one sampling parameter, strategy **i** could be a practical choice.

For cysteine on the gold−thiolate cluster, we obtained the low-energy configurations with only 1000 single-point energy calculations and a few tens of structure optimizations. The number of DFT calculations required is similar to our previous work on gas-phase molecules, again demonstrating the high efficiency of active learning with BOSS. We found that the cysteine on the cluster inherit the conformer types of an isolated cysteine molecule. The whole system is stabilized by both internal hydrogen bonds in cysteine and the H−Au and H−S interactions between the cysteine and the gold−thiolate cluster. However, the cluster environment reorders the energies of the conformer types and enlarges the energy gaps between different configurations.

Our approach is computationally tractable and versatile. The strategies developed in this work to avoid steric clashes are not limited to BO applications. Although we chose a molecule on a cluster as a test system, our approach is suitable for other systems prone to steric clashes, such as long-chain molecules, metal−organic clusters, molecules on nanoparticles, etc. The identified molecular configurations on clusters could also be used as building blocks to construct molecule−metal hybrid clusters such as ligand protected clusters, which we will investigate in future work.

ASSOCIATED CONTENT

Data Availability Statement

The following is a list of software and websites: BOSS, https://gitlab.com/cest-group/boss; FHI-aims, https://fhi-aims.org; data for building GP models with BOSS, https://zenodo.org/record/7012914#.Y72x63bMJaQ; and coordinates of stable local minimum structures, https://nomad-lab.eu/prod/v1/gui/dataset/id/b29x8p2IRSCUtYdbeBFs9A.

Supporting Information

The Supporting Information is available free of charge at https://pubs.acs.org/doi/10.1021/acs.jcim.2c01120.

(Figure S1) Shortest atomic pair distance between the cysteine and the cluster (D_{min}) vs d_1 in system A and system B. (Figure S2) D_{min} vs d_i (i = 2, 3, 4, 5) in system A. (Figure S3) D_{min} vs d_i (i = 2, 3, 4, 5) in system B. (Figure S4) Distribution of the observed energy of system A using strategy **ii** with E_0 = 2.0, 4.0, 6.0 eV. (Figure S5) Distribution of the observed energy of system A using strategy **iii** with E_{cut} = 1.0, 2.0, 3.0 eV. (Figure S6) Convergence information on BOSS hyperparameters length scales for system A with strategies **i**, **ii**, and **iii**. (Figure S7) Convergence information for the global minimum of system A with strategies **i**, **ii**, and **iii**. (Figure S8) Convergence information for the global minimum of system B with strategy **iii**. (PDF)

AUTHOR INFORMATION

Corresponding Author

Xi Chen − *Department of Applied Physics, Aalto University, 00076 AALTO, Finland*; orcid.org/0000-0001-6149-2270; Email: xi.6.chen@aalto.fi

Authors

Lincan Fang − *Department of Applied Physics, Aalto University, 00076 AALTO, Finland*

Xiaomi Guo − *State Key Laboratory of Low Dimensional Quantum Physics and Department of Physics, Tsinghua University, 100084 Beijing, China*

Milica Todorović − *Department of Mechanical and Materials Engineering, University of Turku, FI-20014 Turku, Finland*; orcid.org/0000-0003-0028-0105

https://doi.org/10.1021/acs.jcim.2c01120
J. Chem. Inf. Model. 2023, 63, 745−752

Patrick Rinke − *Department of Applied Physics, Aalto University, 00076 AALTO, Finland;* orcid.org/0000-0003-1898-723X

Complete contact information is available at: https://pubs.acs.org/10.1021/acs.jcim.2c01120

Author Contributions

X.C. and P.R. conceptualized the work. L.F. carried out all the simulations under the supervision of P.R. and X.C. X.G. contributed to the data analysis, and M.T. contributed to the method development. All the authors participated in the manuscript writing.

Notes

The authors declare no competing financial interest.

■ ACKNOWLEDGMENTS

We acknowledge the support from the Academy of Finland (project numbers 308647, 314298, 335571, 316601, and 346377) and COST action CA18234. Generous computational resources were provided by CSC − IT Center for Science, Finland, and the Aalto Science-IT project. L.F. also acknowledges financial support from the Chinese Scholarship Council (Grant No. [2017]3109).

■ REFERENCES

(1) Wang, Y.; Wan, X.-K.; Ren, L.; Su, H.; Li, G.; Malola, S.; Lin, S.; Tang, Z.; Häkkinen, H.; Teo, B. K.; Wang, Q.-M.; Zheng, N. Atomically Precise Alkynyl-Protected Metal Nanoclusters as a Model Catalyst: Observation of Promoting Effect of Surface Ligands on Catalysis by Metal Nanoparticles. *J. Am. Chem. Soc.* **2016**, *138*, 3278−3281.

(2) Maoz, B. M.; Chaikin, Y.; Tesler, A. B.; Bar Elli, O.; Fan, Z.; Govorov, A. O.; Markovich, G. Amplification of Chiroptical Activity of Chiral Biomolecules by Surface Plasmons. *Nano Lett.* **2013**, *13*, 1203−1209.

(3) Wu, Y.; Ali, M. R.; Chen, K.; Fang, N.; El-Sayed, M. A. Gold nanoparticles in biological optical imaging. *Nano Today* **2019**, *24*, 120−140.

(4) Ali, M. R. K.; Wu, Y.; Ghosh, D.; Do, B. H.; Chen, K.; Dawson, M. R.; Fang, N.; Sulchek, T. A.; El-Sayed, M. A. Nuclear Membrane-Targeted Gold Nanoparticles Inhibit Cancer Cell Migration and Invasion. *ACS Nano* **2017**, *11*, 3716−3726.

(5) Azubel, M.; Koivisto, J.; Malola, S.; Bushnell, D.; Hura, G. L.; Koh, A. L.; Tsunoyama, H.; Tsukuda, T.; Pettersson, M.; Häkkinen, H.; Kornberg, R. D. Electron microscopy of gold nanoparticles at atomic resolution. *Science* **2014**, *345*, 909−912.

(6) Zhu, M.; Aikens, C. M.; Hollander, F. J.; Schatz, G. C.; Jin, R. Correlating the Crystal Structure of A Thiol-Protected Au25 Cluster and Optical Properties. *J. Am. Chem. Soc.* **2008**, *130*, 5883−5885.

(7) Baksi, A.; Bootharaju, M. S.; Chen, X.; Häkkinen, H.; Pradeep, T. Ag11(SG)7: A New Cluster Identified by Mass Spectrometry and Optical Spectroscopy. *J. Phys. Chem. C* **2014**, *118*, 21722−21729.

(8) Malola, S.; Nieminen, P.; Pihlajamäki, A.; Hämäläinen, J.; Kärkkäinen, T.; Häkkinen, H. A method for structure prediction of metal-ligand interfaces of hybrid nanoparticles. *Nat. Commun.* **2019**, *10*, 3973−3982.

(9) Hawkins, P. C. D. Conformation Generation: The State of the Art. *J. Chem. Inf. Model.* **2017**, *57*, 1747−1756.

(10) Gronert, S.; O'Hair, R. A. J. Ab Initio Studies of Amino Acid Conformations. 1. The Conformers of Alanine, Serine, and Cysteine. *J. Am. Chem. Soc.* **1995**, *117*, 2071−2081.

(11) Supady, A.; Blum, V.; Baldauf, C. First-Principles Molecular Structure Search with a Genetic Algorithm. *J. Chem. Inf. Model.* **2015**, *55*, 2338−2348.

(12) Vainio, M. J.; Johnson, M. S. Generating Conformer Ensembles Using a Multiobjective Genetic Algorithm. *J. Chem. Inf. Model.* **2007**, *47*, 2462−2474.

(13) Wilke, J. J.; Lind, M. C.; Schaefer, H. F.; Császár, A. G.; Allen, W. D. Conformers of Gaseous Cysteine. *J. Chem. Theory Comput.* **2009**, *5*, 1511−1523.

(14) Rossi, M.; Scheffler, M.; Blum, V. Impact of Vibrational Entropy on the Stability of Unsolvated Peptide Helices with Increasing Length. *J. Phys. Chem. B* **2013**, *117*, 5574−5584.

(15) Chan, L.; Hutchison, G. R.; Morris, G. M. Bayesian optimization for conformer generation. *J. Cheminf.* **2019**, *11*, 32.

(16) Fang, L.; Makkonen, E.; Todorović, M.; Rinke, P.; Chen, X. Efficient Amino Acid Conformer Search with Bayesian Optimization. *J. Chem. Theory Comput.* **2021**, *17*, 1955−1966.

(17) Guo, X.; Fang, L.; Xu, Y.; Duan, W.; Rinke, P.; Todorović, M.; Chen, X. Molecular Conformer Search with Low-Energy Latent Space. *J. Chem. Theory Comput.* **2022**, *18*, 4574−4585.

(18) Jing, B.; Corso, G.; Barzilay, R.; Jaakkola, T. S.Torsional Diffusion for Molecular Conformer Generation. *arXiv Preprint*, arXiv:2206.01729v1, 2022.

(19) Todorović, M.; Gutmann, M. U.; Corander, J.; Rinke, P. Bayesian inference of atomistic structure in functional materials. *npj Comput. Mater.* **2019**, *5*, na.

(20) Ma, X.-Y.; Lyu, H.-Y.; Hao, K.-R.; Zhu, Z.-G.; Yan, Q.-B.; Su, G. High-efficient ab initio Bayesian active learning method and applications in prediction of two-dimensional functional materials. *Nanoscale* **2021**, *13*, 14694−14704.

(21) Zuo, Y.; Qin, M.; Chen, C.; Ye, W.; Li, X.; Luo, J.; Ong, S. P. Accelerating materials discovery with Bayesian optimization and graph deep learning. *Mater. Today* **2021**, *51*, 126−135.

(22) CEST BOSS GitLab project: 16858184. https://gitlab.com/cest-group/boss/ (accessed 2019−03−18).

(23) Akola, J.; Walter, M.; Whetten, R. L.; Häkkinen, H.; Grönbeck, H. On the Structure of Thiolate-Protected Au25. *J. Am. Chem. Soc.* **2008**, *130*, 3756−3757.

(24) Järvi, J.; Rinke, P.; Todorović, M. Detecting stable adsorbates of (1S)-camphor on Cu(111) with Bayesian optimization. *Beilstein J. Nanotechnol.* **2020**, *11*, 1577−1589.

(25) Blum, V.; Gehrke, R.; Hanke, F.; Havu, P.; Havu, V.; Ren, X.; Reuter, K.; Scheffler, M. Ab initio molecular simulations with numeric atom-centered orbitals. *Comput. Phys. Commun.* **2009**, *180*, 2175−2196.

(26) Havu, V.; Blum, V.; Havu, P.; Scheffler, M. Efficient O(N) integration for all-electron electronic structure calculation using numeric basis functions. *J. Comput. Phys.* **2009**, *228*, 8367−8379.

(27) Ren, X.; Rinke, P.; Blum, V.; Wieferink, J.; Tkatchenko, A.; Sanfilippo, A.; Reuter, K.; Scheffler, M. Resolution-of-identity approach to Hartree−Fock, hybrid density functionals, RPA, MP2 and GW with numeric atom-centered orbital basis functions. *New J. Phys.* **2012**, *14*, 053020.

(28) Perdew, J. P.; Burke, K.; Ernzerhof, M. Generalized Gradient Approximation Made Simple. *Phys. Rev. Lett.* **1996**, *77*, 3865.

(29) Tkatchenko, A.; DiStasio, R. A.; Car, R.; Scheffler, M. Accurate and Efficient Method for Many-Body van der Waals Interactions. *Phys. Rev. Lett.* **2012**, *108*, 236402.

(30) Himanen, L.; Geurts, A.; Foster, A. S.; Rinke, P. Data-Driven Materials Science: Status, Challenges, and Perspectives. *Adv. Sci.* **2019**, *6*, 1900808.

(31) Deagen, M. E.; Brinson, L. C.; Vaia, R. A.; Schadler, L. S. The materials tetrahedron has a "digital twin". *MRS Bull.* **2022**, *47*, 379.

(32) The Novel Materials Discovery (NOMAD) Laboratory. Au25cys dataset. DOI: 10.17172/NOMAD/2022.07.19-1 (accessed 2022−07−19).

(33) Sanz, E. M.; Blanco, S.; López, J. C.; Alonso, J. L. Rotational Probes of Six Conformers of Neutral Cysteine. *Angew. Chem., Int. Ed.* **2008**, *47*, 6216−6220.